

Testing Cosmology with Cosmic Sound Waves

Pier Stefano Corasaniti¹ and Alessandro Melchiorri^{2,3}¹LUTH, Observatoire de Paris, CNRS UMR 8102, Université Paris Diderot,
5 Place Jules Janssen, 92195 Meudon Cedex, France²Dipartimento di Fisica e Sezione INFN, Università degli Studi di Roma "La Sapienza", P.le Aldo Moro 5, 00185, Rome, Italy³CERN, Theory Division, CH-1211 Geneva 23, Switzerland

(Dated: April 11, 2013)

WMAP observations have accurately determined the position of the first two peaks and dips in the CMB temperature power spectrum. These encode information on the ratio of the distance to the last scattering surface to the sound horizon at decoupling. However pre-recombination processes can contaminate this distance information. In order to assess the amplitude of these effects we use the WMAP data and evaluate the relative differences of the CMB peaks and dips multipoles. We find that the position of the first peak is largely displaced with the respect to the expected position of the sound horizon scale at decoupling. In contrast the relative spacings of the higher extrema are statistically consistent with those expected from perfect harmonic oscillations. This provides evidence for a scale dependent phase shift of the CMB oscillations which is caused by gravitational driving forces affecting the propagation of sound waves before recombination. By accounting for these effects we have performed a MCMC likelihood analysis of the location of WMAP extrema to constrain in combination with recent BAO data a constant dark energy equation of state parameter w . For a flat universe we find a strong 2 upper limit $w < -1.10$, and including the HST prior we obtain $w < -1.14$, which are only marginally consistent with limits derived from the supernova SNLS sample. On the other hand we infer larger limits for non-flat cosmologies. From the full CMB likelihood analysis we also estimate the values of the shift parameter R and the multipole l_s of the acoustic horizon at decoupling for several cosmologies to test their dependence on model assumptions. Although the analysis of the full CMB spectra should be always preferred, using the position of the CMB peaks and dips provide a simple and consistent method for combining CMB constraints with other datasets.

Keywords: cosmology: observations | CMB

I. INTRODUCTION

Cosmic Microwave Background (CMB) observations have provided crucial insights into the origin and evolution of present structures in the universe [1, 2, 3]. Physical processes occurred before, during and after recombination have left distinctive signatures on the CMB. The most prominent feature is a sequence of peaks and dips in the anisotropy power spectrum, the remnant in prints of acoustic waves propagating in the primordial photon-baryon plasma at the time of decoupling [4, 5, 6]. This oscillatory pattern carries specific information on several cosmological parameters [7]. As an example the angular scale at which these oscillations are observed provides a distance measurement of the last scattering surface to the sound horizon at decoupling, hence a clean test of cosmic curvature [8].

WMAP observations have accurately detected the peak structure of the CMB power spectrum. These data have constrained the geometry of the universe to be nearly flat and have precisely determined other cosmological parameters [9]. On the other hand constraints on dark energy are less stringent, this is because its late time effects leave a weaker in print of the CMB which is diluted by degeneracies with other parameters. Indeed other cosmological tests can be more sensitive to the signature of dark energy, nonetheless they still require additional information from CMB to break the parameter degeneracies. As an example CMB constraints are usu-

ally combined with those from SN Ia luminosity distance data. Alternatively the CMB can be used in combination with measurements of the baryon acoustic oscillations (BAO) in the galaxy power spectrum [10]. In fact the same acoustic signature present in the CMB is also imprinted in the large scale distribution of galaxy, thus providing a complementary probe of cosmic distances at lower redshifts.

A likelihood analysis of the CMB spectra is certainly the more robust approach to implement CMB constraints with those from other datasets. This can be very time consuming, henceforth one can try to compress the CMB information in few measurable and easily computable quantities. Recent literature has focused on the use of the shift parameter R , and the multipole of the acoustic scale at decoupling l_s [11, 12]. However these quantities are not directly measured by CMB observations, they are inferred as secondary parameters from the cosmological constraints obtained from the full CMB likelihood analysis. Consequently their use as data can potentially lead to results which suffer of model dependencies as well as prior parameter assumptions made in the analysis from which the values of R (l_s) have been inferred in the first place. In contrast the multipole location of the CMB extrema can be directly determined from the observed temperature power spectrum through model-independent curve fitting. These measurements can then be used to constrain cosmological parameters provide that pre-recombination corrections are properly

taken into account.

In this paper we analyse in detail the cosmological information encoded in the position of the CMB extrema as measured by WMAP. Our aim is to provide a simple and unbiased method for incorporating CMB constraints into other datasets which is alternative to that of using R and/or ℓ_b [11, 12]. Firstly we estimate the amplitude of pre-recombination mechanisms that can displace the location of the CMB extrema with the respect to the angular scale of the sound horizon at decoupling. In particular we show that the WMAP location of the first peak is strongly affected by such mechanisms, while the displacements induced on the higher peaks and dips are smaller. By accounting for these effects we perform a cosmological parameter analysis and infer constraints on dark energy under different prior assumptions, including the cosmic curvature. We then combine these results with measurements of BAO from SDSS and 2dF data [13], and confront the inferred constraints with those obtained using SN Ia data from the Supernova Legacy Survey [14]. Finally we test for potential model dependencies of R (and ℓ_b) by performing a full likelihood analysis of the WMAP spectra for different sets of cosmological parameters.

The paper is organized as follows: in Section II we review the physics of the CMB acoustic oscillations. In Section III we discuss the relative shifts of the multipoles of the WMAP peaks and dips. In Section IV we present the results of the cosmological parameter inference using the location of the CMB extrema in combination with BAO. In Section V we confront the results with the SN Ia likelihood analysis from the SNLS sample. We discuss the results on the shift parameter in Section VI and present our conclusions in Section VII.

II. CMB ACOUSTIC OSCILLATIONS

The onset of acoustic waves on the sub-horizon scales of the tightly coupled photon-baryon plasma before recombination is natural consequence of photon pressure resisting gravitational collapse. The properties of these oscillations depends both on the background expansion and the evolution of the gravitational potentials associated with the perturbations present in the system. In the following we will briefly review the basic processes which affect the propagation of these waves before decoupling. Interested readers will find more detailed discussions in [6, 7]. Let consider the photon temperature fluctuation δT (monopole), following Hu and Sugiyama [6] its evolution is described by

$$\ddot{\delta T} + \frac{R}{1+R} \dot{\delta T} + k^2 c_s^2 \delta T = F(\ell); \quad (1)$$

where the dot is the derivative with respect to conformal time, $R = 3 \rho_b / 4 \rho_\gamma$ is the baryon-to-photon ratio, k is the wavenumber, $c_s = c / \sqrt{3(1+R)}$ is the sound speed of the system with c the speed of light. The source term

$$F = \frac{R}{1+R} \ddot{\delta \Phi} - k^2 \frac{1}{3} \delta \Phi; \quad (2)$$

represents a driving force, where $\delta \Phi$ and $\delta \Psi$ are the gauge-invariant metric perturbations respectively.

It is easy to see from Eq. (1) that the homogeneous equation ($F = 0$) admits oscillating solutions of the form,

$$\delta T_{\text{hom}}(\ell) = A_1 \cos k r_s(\ell) + \frac{A_2}{k} \sin k r_s(\ell) \quad (3)$$

where A_1 and A_2 are set by the initial conditions and $r_s(\ell) = \int_0^{\ell} c_s(\ell') d\ell'$ is the sound horizon at time ℓ . At time of decoupling ℓ_{dec} , the positive and negative extrema of these oscillations appear as a series of peaks in the anisotropy power spectrum. Their location in the multipole space is a multiple integer of the inverse of the angle subtended by the sound horizon scale at decoupling, namely $\ell_{\text{peak}}^{\text{peak}} = m \ell_b$ with $m = 1; 2; \dots$ and

$$\ell_b = \frac{r_K(z)}{r_s(z)}; \quad (4)$$

where z is the recombination redshift and $r(z)$ the comoving distance to z ,

$$r_K(z) = \frac{c}{H_0} \int_{j_K}^1 \frac{1}{j_K} f\left(\frac{1}{j_K}\right) I(z); \quad (5)$$

with H_0 the Hubble constant, $j_K = 1/K = H_0^2$ with K the constant curvature, $f(x) = \sin(x); \sinh(x); x$ for $K > 0; < 0$ and $= 0$ respectively, and $I(z) = \int_0^z dz' H_0 = H(z^0)$.

Scales for which the monopole vanishes also contribute to anisotropy power spectrum. In such a case the signal comes from the non-vanishing photon velocity v_1 (dipole) which oscillates with a phase shifted by $\pi/2$ with the respect to the monopole [6]. Therefore photons coming from these regions are responsible for a series of troughs in the anisotropy power spectrum at multipoles $\ell_{\text{dip}}^{\text{dip}} = n \ell_b$ with $n = m + 1 = 2$.

The full solution to Eq. (1) at decoupling reads as [15]:

$$\delta T(\ell) = \delta T_{\text{hom}}(\ell) + \frac{A_3}{k} \int_0^{\ell} d\ell' [1 + R(\ell')]^{3/4} \sin[k r_s(\ell) - k r_s(\ell')] F(\ell'); \quad (6)$$

where A_3 is set by the initial conditions. As we can see from Eq. (6) including the driving force F induces a scale dependent phase shift of the acoustic oscillations, which is primarily caused by the time variation of the gravitational potential. In fact perturbations on scales which enter the horizon at the matter-radiation equality experience a variation of the expansion rate which causes a time evolution of the associated gravitational potentials. This mechanism is dominant on the large scales and is responsible for the so called early Integrated Sachs-Wolfe (ISW) effect [16]. The overall effect is to displace the acoustic oscillations with the respect to the pure harmonic series. For a spectrum of adiabatic perturbations we may expect this displacement to become negligible on higher harmonics since the gravitational potentials decay as $\propto (k)^{-2}$ on scales well inside the horizon. This is not the case if active perturbations were present on such scales before the epoch of decoupling.

In order to account for these pre-recombination effects a realistic modeling of the multipole position of the CMB maxima and minima is given by [17]

$$l_m = l_a(m, \delta'_m); \quad (7)$$

where $m = 1; 2; \dots$ for peaks, and $m = 3; 2; 5; 2; \dots$ for dips; δ'_m parameterizes the displacement caused by the driving force. Because of the scale dependent nature of the driving effect discussed above, it is convenient to decompose the correction term as $\delta'_m = \delta'_1 + \delta'_m$, where δ'_1 is the overall shift of the first peak with respect to the sound horizon, and δ'_m is the shift of the m -th extrema relative to the first peak [18].

It is worth noticing that while the position of the CMB extrema depends through l_a on the geometry and late time expansion of the universe, their relative spacing depends through δ'_m only on pre-recombination physics.

III. PHASE SHIFT OF WMAP PEAKS AND DIPS

WMAP observations have provided an accurate determination of the CMB power spectrum. The multipoles of the CMB extrema have been inferred using a functional fit to the uncorrelated band powers as described in [19]. Hinshaw et al. [3] have applied this method to the WMAP-3yr data and found the position of the first two peaks and dips to be at $l_1 = 220.8 \pm 0.7$, $l_{3=2} = 412.4 \pm 1.9$, $l_2 = 530.9 \pm 3.8$ and $l_{5=2} = 675.2 \pm 11.1$ respectively.

We want to determine whether these measurements provide any evidence for driving effects affecting the acoustic oscillations. In order to do so we evaluate the relative spacings between the WMAP measured m -th and m^0 -th extrema,

$$\Delta_{l, m^0} = \frac{l_m - l_{m^0}}{l_{m^0}} \quad 1; \quad (8)$$

and the propagated errors $\sigma_{\Delta_{l, m^0}}$.

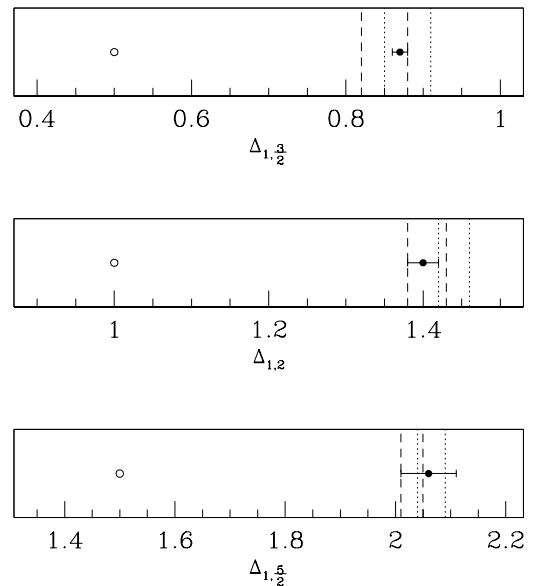


FIG. 1: WMAP spacings of $l_{3=2}$, l_2 and $l_{5=2}$ relative to l_1 (black solid circles) and propagated errors. The values expected from the harmonic series are $\Delta_{l, 3=2} = 1=2$, $\Delta_{l, 2} = 1$ and $\Delta_{l, 5=2} = 3=2$ (open circles). Vertical dashed lines delimit the expected interval of variation of the relative spacings obtained by including the shift corrections as parameterized in [18] and evaluated over a conservative range of cosmological parameter values (see text). The dotted vertical lines include the effect of three massless neutrinos.

Let us first consider the spacings relative to the location of the first peak. We find $\Delta_{l, 3=2} = 0.87 \pm 0.01$, $\Delta_{l, 2} = 1.40 \pm 0.02$ and $\Delta_{l, 5=2} = 2.06 \pm 0.05$ respectively. These estimates are shown in Figure 1 (black solid circles), where we also plot the relative spacings as expected from a sequence of perfect acoustic oscillations (open circles). It is evident that the WMAP inferred values of $\Delta_{l, m}$ lie many sigma away from those expected from the harmonic series. This provides clear evidence that the position of the first peak is largely affected by the driving force at decoupling. Such a large displacement is most likely caused by the early ISW, although an additional contribution from isocurvature fluctuations [20] or active gravitational potentials [21] cannot be excluded.

Let us focus now on the displacement of the second peak relative to the first one, since $\Delta_{l, 2} > 1$ it follows that $\delta'_1 > \delta'_2$. This implies that the overall shift of l_1 with respect to l_a is larger than the shift of l_2 relative to l_1 . As discussed in the previous section this is consistent with having the gravitational potentials inside the sound horizon scaling as $\propto (k)^{-2}$, thus inducing a weaker driving force. This can be seen more clearly in Figure 2 where we plot $\Delta_{l, 3=2, 2}$, $\Delta_{l, 2, 5=2}$ and $\Delta_{l, 3=2, 5=2}$.

Apart $\Delta_{l, 2, 3=2} = 0.29 \pm 0.01$, whose value suggests the presence of a non-negligible driving effect still on the scale of the first dip, we may notice that all other spacings

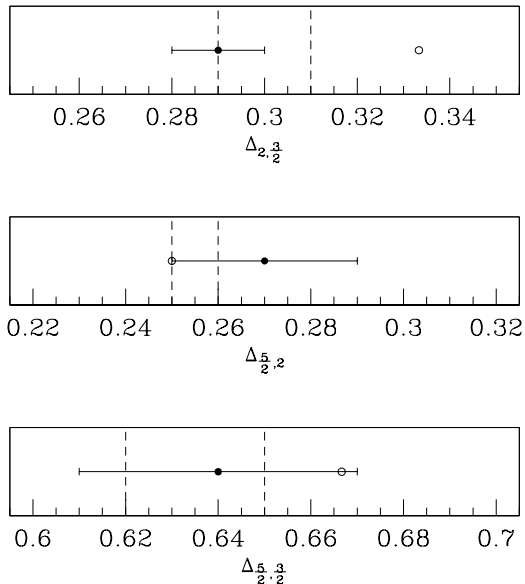


FIG. 2: As in Figure 1 for $l_{3=2}$, l_2 and $l_{5=2}$ relative spacings. The harmonic series values are $l_{3=2;2} = 1=3$, $l_{2;5=2} = 1=4$ and $l_{3=2;5=2} = 2=3$.

are statistically consistent with the prediction of the harmonic series.

Therefore these results suggest the existence of a scale dependent phase shift of the CMB acoustic oscillations. The effect is larger on the scale of the first acoustic peak, while it is weaker for the higher harmonics. The upcoming Planck mission will map more accurately the location of the higher peaks and dips and provide a cleaner detection of this shift.

Indeed driving effects are well accounted for by the CMB theory as incorporated in standard Boltzmann codes [22]. For instance a standard adiabatic spectrum of initial density perturbations leads to phase shifts which are consistent with those we have inferred here. To show this we have used the fitting formulas provided in [18] for adiabatic models which parametrize δ'_m in terms of the total matter density $\delta_m h^2$, the baryon density $\delta_b h^2$, the dark energy density at decoupling δ_{DE}^{dec} and the scalar spectral index n_s . Assuming $\delta_{DE}^{\text{dec}} = 0$ we evaluate these formulas over the following range of parameter values, $0.08 < \delta_m h^2 < 0.11$, $0.020 < \delta_b h^2 < 0.024$, $0.92 < n_s < 1.1$ and infer the corresponding intervals for the relative spacings $\delta_{m,m}$. These are drawn in Figure 1 and 2 as vertical dashed lines. It can be seen that these intervals are statistically consistent with the measured spacings. Including the contribution of three massless neutrinos (dotted vertical lines) slightly shifts the $l_{1,m}$ intervals further from the expected values of the perfect harmonic oscillator. This is because the presence of relativistic neutrinos extend the radiation era and therefore leads to a more effective early ISW effect on the large

scales. In contrast we find no differences for the intervals of the other peaks and dips spacings.

IV. PARAMETER INFERENCE

We perform a Markov Chain Monte Carlo (MCMC) likelihood analysis to derive cosmological parameter constraints using the measurements of the WMAP extrema discussed in the previous section. Again we account for the shift corrections by evaluating the model prediction for l_m using Eq. (7), with the displacements δ'_m parametrized as in [18]. We compute the recombination redshift z using the fitting formulae provided in [23]. Cosmological constraints derived from the location of the CMB peaks have been presented in previous works (e.g. [24, 25, 26]). Here our aim is to derive bounds on dark energy which are independent of Supernova Ia data and rely only on the cosmic distance information encoded in the angular scale of the sound horizon as inferred from the multipole position of the WMAP peaks and dips, and BAO measurements.

First we consider flat models with dark energy parametrized by a constant equation of state w . We then test the stability of the inferred constraints by extending the analysis to models with non-vanishing curvature, $\Omega_k \neq 0$. We also consider flat dark energy models with a time varying equation of state parametrized as $w = w_0 + w_1(1 - a)$ (CPL) [27, 28]. We want to remark that for models with $w_1 \neq 1$, the dark energy density can be non-negligible at early times. Therefore in order to consistently account for the shifts induced on the location of the CMB peaks and dips, we compute for each model in the chain the corresponding value of δ_{DE}^{dec} so as to include its value in the shift fitting formulae.

The credible intervals on the parameters of interest are inferred after marginalizing over h , $\delta_b h^2$ and n_s respectively. We let them vary in the following intervals: $0.40 < h < 1.00$, $0.020 < \delta_b h^2 < 0.024$ and $0.94 < n_s < 1.10$. Marginalizing over these parameters is necessary due to the parameter degeneracies in r_K , r_s and to properly account for the shift corrections δ'_m .

As complementary dataset we use the cosmic distance as inferred from the BAO in the SDSS and 2dF surveys [13]. These measurements consists of the ratio $r_s(z) = D_V(z)$, where $D_V(z)$ is a distance measure given by

$$D_V(z) = (1+z)^2 D_A(z) c z = H(z)^{-1=3}; \quad (9)$$

with $D_A(z) = r_K(z)/(1+z)$ the angular diameter distance at z . In particular Percival et al. [13] have found, $D_V(0.35) = D_V(0.2) = 1.812 \pm 0.060$.

In order to reduce the degeneracy with the Hubble parameter we also infer constraints assuming a Gaussian HST prior $h = 0.72 \pm 0.08$ [29]. In Figure 3 we plot the marginalized 1 and 2 contours in the $\delta_m - w$, $w - \Omega_k$ and $w_0 - w_1$ respectively. The upper panels correspond to constraints inferred from WMAP extrema alone, while the

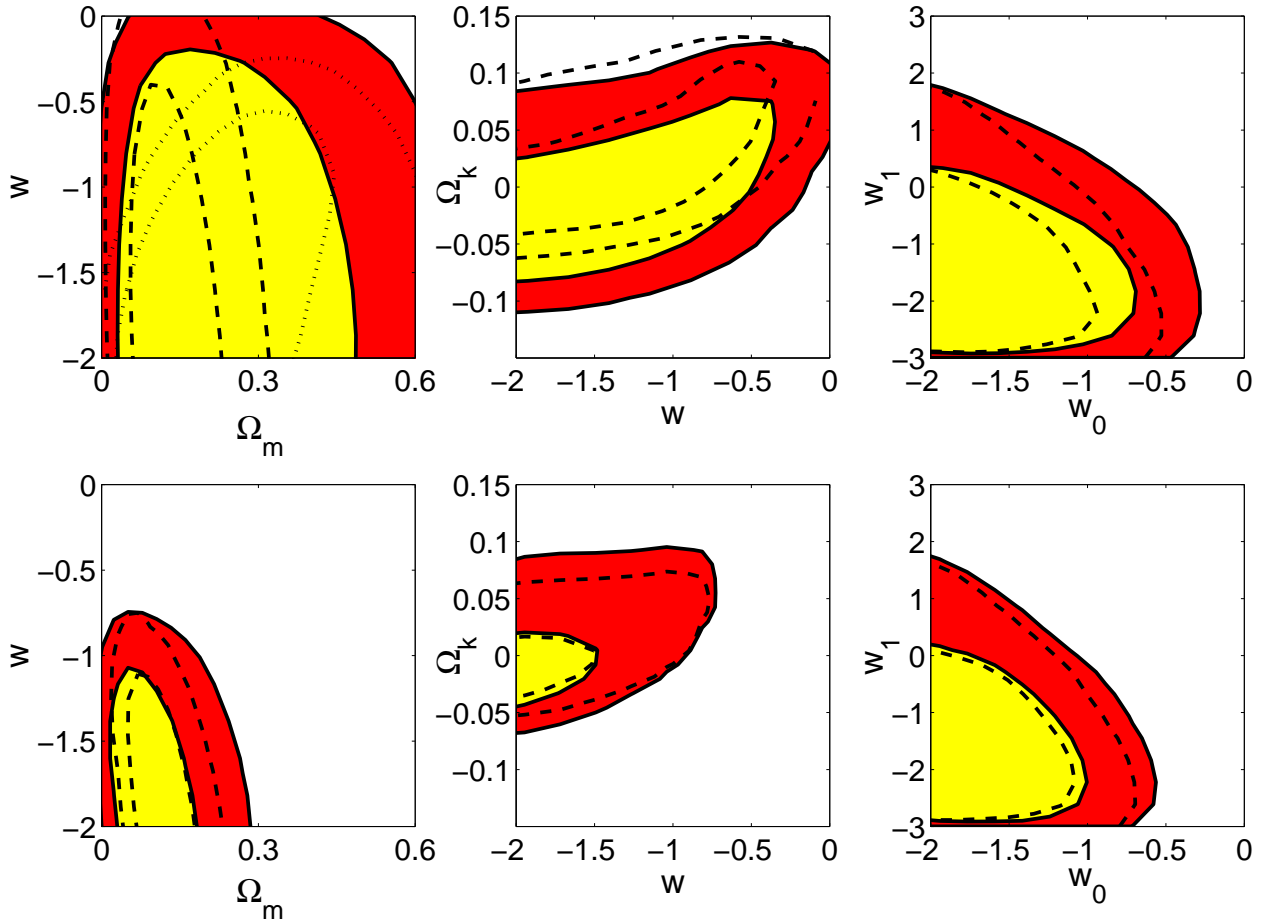


FIG. 3: Marginalized 1 and 2 likelihood contours from WMAP extrema (upper panels) and in combination with BAO (lower panels). Dashed lines correspond to contours inferred under HST prior. The dotted lines in the upper left panel correspond to limits inferred assuming $\Omega_b = 0.023$ and $n_s = 0.96$.

lower panels include the BAO data. Dashed contours are inferred under the HST prior. To be conservative we only quote marginalized 2 limits. We now discuss these results in more detail.

A. Limits from CMB peaks and dips

As it can be seen in Figure 3 (upper left panel) the CMB extrema alone poorly constrain the Ω_m - w plane. In particular the 1 and 2 regions are larger than those obtained from the WMAP analysis [9]. This is because due to the late ISW effect more information about dark energy is contained in the full CMB spectrum than just in the distance to the last scattering surface as encoded in the position of the CMB peaks and dips. Besides several degeneracies with other parameters are strongly reduced. A direct consequence of this is that our limits on w are unbounded from below. After marginalizing over all parameters we find $\Omega_m = 0.29^{+0.41}_{-0.23}$ and $w < 0.18$ at 2 σ . A model with $\Omega_m = 1$ is consistent at 95% confidence level with the location of the WMAP extrema provided

that $h = 0.42$. This is in agreement with the results presented in [30]. On the other hand in posing an HST prior (dash contours) reduce the degeneracy in the Ω_m - w plane, and the marginalized 2 limits are $\Omega_m = 0.16^{+0.15}_{-0.11}$ and $w < 0.25$ respectively. The upper limit on w improves if a strong prior on $\Omega_b h^2$ and n_s is assumed (dotted contours in the upper left panel). As an example in posing $\Omega_b h^2 = 0.0223$ and $n_s = 0.96$, we find $w < 0.65$ at 2 σ . Indeed using the analysis of the full CMB power spectrum provides better constraints. For instance in Fig. 4 we plot the 1 and 2 contours inferred from a MCMC likelihood analysis of the WMAP-3yrs spectra in combination with the HST prior. The limits are more stringent than in the previous case. This is because the amplitude of the first peak as well as the relative amplitude of the other peaks are particularly sensitive to Ω_m , Ω_b and h . Hence degeneracies contributing to the uncertainties in the Ω_m - w plane are further reduced. As mentioned before, a robust dark energy parameter inference needs the analysis of the full CMB spectrum. However in the case one aims to infer constraints from other datasets such as SN Ia or BAO and include CMB information in

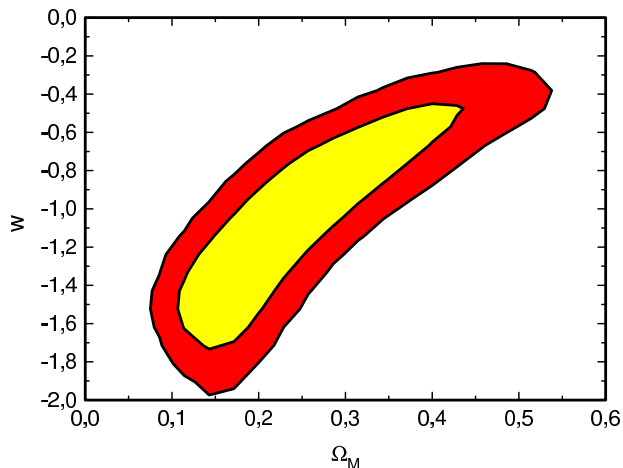


FIG. 4: Marginalized 1 and 2 likelihood contours inferred from the full WMAP-3yrs spectra.

a rapid and simple manner, the position of the CMB extrema provides a very efficient tool. In fact while the CMB power spectrum analysis requires the solution of the Boltzmann equation for a given cosmological model, the evaluation of the position of the CMB peaks and dips only is a semi-analytical computation. As an example running publicly available Boltzmann codes [22] on a CPU at 2.3GHz requires about one minute to compute the spectra of a single model, and even using a MCMC sampling the overall likelihood analysis still require about one hour to reach full convergence of the MCMC chains, while using the CMB extrema only takes few minutes.

In Fig. 3 (central upper panel) we extend our analysis of the CMB peaks and dips to non-flat models. Allowing for a non-vanishing curvature increases the geometric degeneracy and consequently leads to larger uncertainties in w . For instance the 2 marginalized constraints are $w < 0.34$ and $\kappa = 0.01 - 0.05$ respectively, and do not improve significantly under the HST prior.

The position of the CMB peaks and dips alone does not provide any insight on the time variation of dark energy. As it can be seen in Fig. 3 (right upper panel) the contours in the w_0 - w_1 plane are spread over a large range of values. After marginalizing we find $w_0 < 0.55$ and $w_1 < 1.68$ at 2. It is worth mentioning that for increasing values of w_1 , dark energy becomes dominant at earlier times. In such a case the presence of a non-negligible dark energy density at recombination modifies the position of the CMB peaks and dips primarily through its effect on the size of the sound horizon at decoupling. Therefore the location of the CMB extrema (after having accounted for the relative shifts) can put an upper bound on the time evolution of the equation of state at high redshifts (i.e. w_1). Our analysis shows that in order to be consistent with the observed peak structure, large positive values of $w_1 > 1$ are excluded (see also Section V). This is consistent with the fact that the analysis of the full CMB spectrum limits the amount of dark energy density

at recombination to be less than 10% (otherwise it would strongly affect the amplitude and location of the CMB Doppler oscillations), hence providing a stringent upper bounds on the value of the dark energy equation of state at early time (see [31, 32]). In contrast models with large negative values of $w_1 < 0$ leave no imprint at high redshifts, since in this case the dark energy density rapidly decreases for $z > 0$. Consequently the likelihood remains unbounded in this region of the parameter space.

B. Combined constraints from CMB extrema and BAO

The baryon acoustic oscillations in the galaxy power spectrum provide a cosmic distance test at low redshifts. Therefore in combination with CMB measurements they can significantly reduce the cosmological parameter degeneracies. In Fig. 3 (lower left panel) we plot the combined 1 and 2 contours in the Ω_m - w plane. At 95% confidence level we find $\Omega_m = 0.12 - 0.12$ and $w < -1.10$ respectively. Imposing the HST prior further constrains the dark energy equation of state, $w < -1.14$. These results are compatible with those found in [13]. A model with $\Omega_m = 1$ is now excluded with high confidence level since the combination of CMB extrema and BAO constrain the Hubble parameter in the range $h = 0.71 - 0.20$ at 2 (see also [30]). Interestingly the CDM case ($w = -1$) appears to be on the edge of the 2 limit, hence favoring non-standard dark energy models. Indeed unaccounted systematic effects in the BAO data can be responsible for such super-negative values of w . On the other hand if confirmed this would provide evidence for an exotic phantom dark energy component [33] or interpreted as the cosmological signature of a dark sector interactions (e.g. [34]).

The credible regions for non-flat models are shown in Fig. 3 (central lower panel). In this case we find $\kappa = 0.011 - 0.064$ and $w < 0.46$ at 2. These bounds do not change significantly under the HST prior. In Fig. 3 (lower right panel) we plot the 1 and 2 contours in the w_0 - w_1 plane. Also in this case the bounds on a time varying dark energy equation of state remain large. For instance we find the marginalized 2 limits to be $w_0 < 0.74$ and $w_1 < 1.6$. Necessarily inferring tighter bounds on w_1 will require the combination of several other datasets such as SN Ia luminosity distance measurements [35], which is the topic of next Section.

V. CONSTRAINTS FROM SN IA

Here we want to compare the results derived in the previous Section with limits inferred from luminosity distance measurements to SN Ia. We use the SN dataset from the Supernova Legacy Survey (SNLS) [14], and for simplicity we limit our analysis to flat models. The results are summarized in Fig. 5 and Fig. 6 where we plot

the 1 and 2 contours in the $\Omega_m - w$ and $w_0 - w_1$ planes respectively. The shaded regions correspond to limits inferred by combining the SN data with the location of the CMB extrema and assuming a hard prior on the baryon density and the scalar spectral index, $n_b = 0.023$ and $n_s = 0.96$ respectively. We have verified that the constraints do not change significantly assuming different prior parameter values.

Let us first focus on Fig. 5. We can see that the degeneracy line in the $\Omega_m - w$ plane is almost orthogonal to that probed by CMB and BAO, and indeed using the SN data requires external information to extract tighter constraints on dark energy. A common procedure is to assume a Gaussian prior on Ω_m consistently with the parameter inference from CMB and large scale structure measurements, or alternatively to combine the SN analysis with BAO or the CMB shift parameter. Here we derive limits by combining the SN data with the position of the CMB peaks and dips. This breaks the parameter degeneracy, thus providing smaller "credible" contours (shaded contours). In particular after marginalizing, we find $\Omega_m = 0.24 \pm 0.11$ and $w = 1.01 \pm 0.29$ at 2 respectively. We can notice that these limits are only marginally consistent with those inferred using BAO in the previous Section, thus indicating a potential discrepancy between the BAO measurements obtained in [13] and the SNLS data [14].

Let us now consider the case of a time varying equation of state. It is obvious that the parameter degeneracy between the matter density and the dark energy equation of state is increased when additional equation of state parameters which accounts for a possible redshift dependence are included in the data analysis. This can be clearly seen in Fig. 6 where we plot the 1 and 2 contours in the $w_0 - w_1$ plane. Nevertheless the SN data, differently from the case of BAO data in combination with CMB extrema (see lower left panel in Fig. 3), constrain w_0 in a finite interval. This is because SN Ia observations by testing the luminosity distance over a range of redshift where the universe evolves from a matter dominated expansion to one driven by dark energy, are sensitive to at least one dark energy parameter (i.e. w or w_0) [36]. In such a case adding external information breaks the internal degeneracy and leads to finite bounds on both dark energy parameters. For instance including the position of the CMB peaks and dips, the root-mean-square value and standard deviation for w_0 and w_1 derived from the MCMC chains are $w_0 = 1.04 \pm 0.33$ and $w_1 = 0.27 \pm 2.27$ respectively; the best fit model being $w_0 = 1.02$ and $w_1 = 0.04$. These results are consistent with those from other analysis in the literature (see e.g. [12]).

V I. S H I F T P A R A M E T E R

The geometric degeneracy of the CMB power spectrum implies that different cosmological models will have sim-

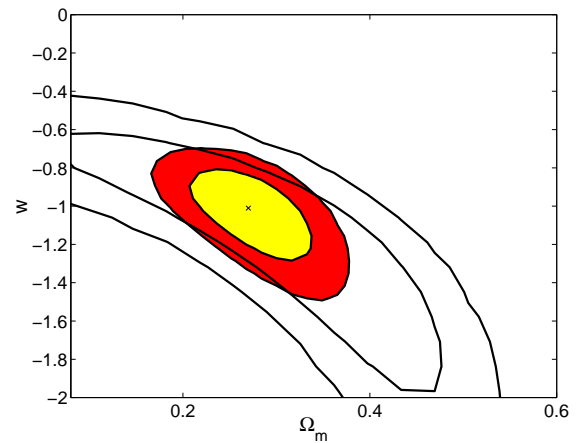


FIG. 5: Marginalized 1 and 2 contours in the $\Omega_m - w$ plane from SNLS data (solid lines) and in combination with the location of the CMB extrema (red and yellow shaded regions).

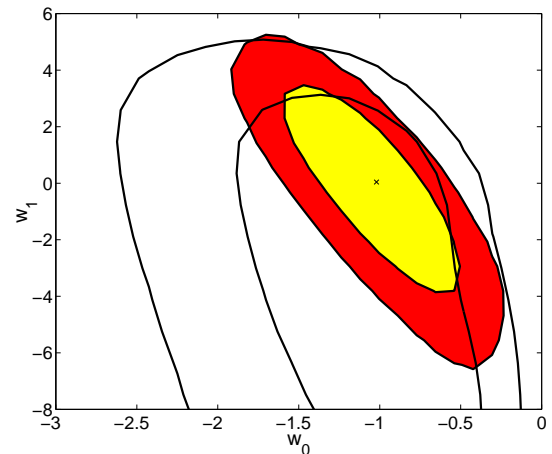


FIG. 6: As in Figure 5 in the $w_0 - w_1$ plane.

ilar spectra if they have nearly identical matter densities $\Omega_m h^2$ and $\Omega_b h^2$, primordial spectrum of fluctuations and shift parameter $R = \frac{p}{\Omega_m H_0^2 r_K(z)}$ [37]. The authors of [12] have suggested that since Ω_b is nearly uncorrelated with R , then both parameters can be used to further compress CMB information and combined with other measurements in a friendly user manner. For a minimal extension of the dark energy parameters the inferred values of R and Ω_b do not significantly differ from those inferred assuming the vanilla Λ CDM model [11, 12]. Indeed differences may arise if additional parameters, such as the neutrino mass, the running of the scalar spectral index or tensor modes are considered [11]. We extend this analysis to other models. In particular by running a MCMC likelihood analysis of the full WMAP-3yrs spectra we infer constraints on R and Ω_b for models with an extra-background of relativistic particles (characterized by the number of relativistic species $N_{\text{eff}} \notin 3$) [38], neutrino mass [39], a time varying equation of state parameterized in the form of CPL, and a dark energy component with

M odel	R	l_b
CDM	1:707 0:025	302:3 1:1
wCDM ($c_{D,E}^2 = 1$)	1:710 0:029	302:3 1:1
wCDM ($c_{D,E}^2 = 0$)	1:711 0:025	302:4 1:1
CDM $m > 0$	1:769 0:040	306:7 2:1
CDM $N_{eff} \notin 3$	1:714 0:025	304:4 2:5
CDM $k \notin 0$	1:714 0:024	302:5 1:1
w(z)CDM CPL ($c_{D,E}^2 = 1$)	1:710 0:026	302:5 1:1
CDM + tensor	1:670 0:036	302:0 1:2
CDM + running	1:742 0:032	302:8 1:1
CDM + running + tensor	1:708 0:039	302:8 1:2
CDM + features	1:708 0:028	302:2 1:1

TABLE I: The 68% C.L. limits on the shift parameter R and the acoustic scale derived from the WMAP data. A top-hat age prior $10 \text{ G yrs} < t_0 < 20 \text{ G yrs}$ is assumed.

perturbations characterized by the sound speed $c_{D,E}^2$. We also consider models with a running of the scalar spectral index, with a non-vanishing tensor contribution (see e.g. [40]) and, finally, with extra-features in the primordial spectrum due to a sharp step in the in situ potential as in [41].

As we can see from Table I the constraints on R and l_b are stable under minimization of the dark energy model parameters, differences are smaller than few per cent including the case of a clustered dark energy component ($c_{D,E}^2 = 0$). In contrast the confidence interval of l_b is shifted by few per cent in the CDM model with the neutrino mass or an extra background of relativistic particles, while the values of R are slightly modified for a running of the primordial power spectrum or the contribution of tensor modes. These results confirm previous analysis [11, 12].

Although the values of R and l_b are nearly the same for the dark energy models we have considered, this should not be considered as an incentive to use these parameters without caution. For instance there is no specific reason as to why one should use the values of R and l_b inferred from the vanilla CDM, rather than those obtained accounting for the neutrino mass. Consequently one may infer slightly different bounds on the dark energy parameters depending whether neutrinos are assumed to be massless or not. Moreover the fact that WMAP data constrain R and l_b to be nearly the same for simple dark energy models is because the effect of dark energy on the epoch of matter-radiation equality and the evolution of the density perturbations remains marginal. This might not be the case for other models, such as those for which the dark energy density is a non-negligible at early times. Since this effect is not accounted for in the values of R and l_b inferred from the vanilla CDM, their use may lead to strongly biased results. In contrast the location of the CMB extrema is applicable to this class of models as well [18]. A similar consideration applies to inhomogeneous models in which the late times dynamics and geometry departs from that of the standard FRW universe [42].

The applicability to models of modified gravity, such

as the DGP scenario [43] deserves a separate comment. In these models not only the Hubble law differs from the standard CDM, but also the evolution of the density perturbations can be significantly different. Therefore unless the evolution of the linear perturbations is understood well enough as to allow for a precise calculation of the CMB and matter power spectra, the use of R and l_b , or alternatively of the position of the CMB extrema or the distance measurements from BAO might expose to the risk of completely wrong results.

VII. CONCLUSIONS

The multipoles of the CMB extrema can be directly measured from the WMAP spectra and used to combine CMB information with other cosmological datasets. Corrections to the location of the CMB peaks and dips from pre-recombination effects need to be taken into account for an unbiased parameter inference. Here we have shown that the position of the first peak as measured by WMAP-3yrs data is strongly displaced with the respect to the actual location of the acoustic horizon at recombination. This displacement is caused by gravitational driving forces affecting the propagation of sound waves before recombination. These effects are smaller on higher harmonics, indicating the presence of a scale dependent phase shift which becomes negligible on scales well inside the horizon.

We have performed a cosmological parameter inference using the position of the WMAP peaks and dips in combination with recent BAO measurements and derived constraints on a constant dark energy equation of state under different model parameter assumptions.

The method we have presented here is alternative to using the shift parameter R and/or the multipole of the acoustic horizon at decoupling l_b . We have tested for potential model dependencies of R and l_b by running a full CMB spectra likelihood analysis for different class of models. Indeed for simple dark energy models the inferred constraints on R and l_b do not differ from those inferred assuming the vanilla CDM. Nevertheless we have suggested caution in using these secondary parameters as data, since hidden assumptions may lead to biased results particularly when testing models which greatly depart from the CDM cosmology.

Indeed we do advocate the use of the full CMB spectra, particularly for constraining the properties of dark energy. In fact more information on dark energy is encoded in the full CMB spectrum than just in the distance to the last scattering surface. Nevertheless we think that using the location of the CMB extrema provide a fast and self-consistent approach for combining in a friendly user way the CMB information with complementary cosmological data.

A cknow ledgm ents

PSC is grateful to the Aspen Center for Physics for the hospitality during the "Supernovae as Cosmological Distance Indicators" Workshop where part of this work has been developed. We are particularly thankful to

Jean-Michel Alimi, Laura Covi, Michael Doran, Malcolm Fairbairn, Jan Hamann, Martin Kunz, Julien Larena, Eric Linder, Yun Wang and Martin White for discussions, suggestions and help. We acknowledge the use of CosmoMC [44] for the analysis of the MCMC chains.

-
- [1] P. De Bernardis et al., *Nature*, 404, 955 (2000); N. W. Halverson et al., *Astrophys. J.*, 568, 38 (2002)
- [2] M. C. R. Unyan et al., *New Astron. Rev.*, 47, 915 (2003); C. L. Bennett et al., *Astrophys. J. Supp.*, 148, 1 (2003)
- [3] G. H. Inshaw et al., *Astrophys. J. Supp.*, 170, 288 (2007)
- [4] A. D. Sakharov, *JETP*, 49, 345 (1965); J. Silk, *Astrophys. J.*, 151, 459 (1968); P. J. E. Peebles and I. T. Yu, *Astrophys. J.*, 162, 815
- [5] N. Vittorio and J. Silk, *Astrophys. J. Lett.*, 285, 39 (1984); J. R. Bond and G. Efstathiou, *Astrophys. J. Lett.*, 285, 45 (1984); A. G. Doroshkevich, *Sov. Astron. Lett.*, 14, 125 (1988)
- [6] W. Hu and N. Sugiyama, *Phys. Rev. D* 51, 6 (1995);
- [7] W. Hu and M. White, *Astrophys. J.*, 471, 30 (1996)
- [8] M. Kamionkowski, D. N. Spergel and N. Sugiyama, *Astrophys. J. Lett.*, 426, 57 (1994)
- [9] D. N. Spergel et al., *Astrophys. J. Supp.*, 170, 377 (2007)
- [10] D. J. Eisenstein, W. Hu and M. Tegmark, *Astrophys. J. Lett.*, 504, 57 (1998)
- [11] O. Elgaroy and T. Multamaki, *Astron. & Astrophys.*, 471, 65 (2007)
- [12] Y. Wang and P. Mukherjee, *astro-ph/0703780*
- [13] W. J. Percival et al., *arXiv:0705.3323*
- [14] P. Astier et al., *Astron. & Astrophys.*, 447, 31 (2006)
- [15] W. Hu and N. Sugiyama, *Astrophys. J.*, 444, 489 (1995)
- [16] M. J. Rees and D. W. Sciama, *Nature*, 217, 511 (1968)
- [17] W. Hu, M. Fukugita, M. Zaldarriaga and M. Tegmark, *Astrophys. J.*, 549, 669 (2001)
- [18] M. Doran and M. Lilley, *Mont. Not. Roy. Astron. Soc.*, 330, 965 (2002)
- [19] L. Page et al., *Astrophys. J. Supp.*, 148, 233 (2003)
- [20] R. Keskitalo et al., *J. Cosmol. Astropart. Phys.*, 09, 008 (2007)
- [21] J. Magueijo et al., *Phys. Rev. Lett.*, 76, 15 (1996)
- [22] U. Seljak and M. Zaldarriaga, *Astrophys. J.*, 469, 437 (1996); A. Lewis, A. Challinor and A. Lasenby, *Astrophys. J.* 538, 473 (2000); M. Doran, *J. Cosmol. Astropart. Phys.*, 10, 011 (2005)
- [23] W. Hu and N. Sugiyama, *Astrophys. J.*, 471, 542 (1996)
- [24] P. S. Corasaniti and E. J. Copeland, *Phys. Rev. D* 65, 043004 (2002)
- [25] M. Doran, M. Lilley and C. Wetterich, *Phys. Lett. B* 528, 175 (2002)
- [26] S. Sen and A. A. Sen, *Astrophys. J.*, 588, 1 (2003)
- [27] M. Chevallier and D. Polarski, *Int. J. Mod. Phys. D* 10, 213 (2001)
- [28] E. V. Linder, *Phys. Rev. Lett.* 90, 091301 (2003)
- [29] W. L. Freedman et al., *Astrophys. J.*, 553, 47 (2001)
- [30] P. Hunt and S. Sarkar, *arXiv:0706.2443*
- [31] R. R. Caldwell and M. Doran, *Phys. Rev. D* 69, 103517 (2003);
- [32] P. S. Corasaniti et al., *Phys. Rev. D* 70, 083006 (2004);
- [33] R. R. Caldwell, M. Kamionkowski, N. Weinberg, *Phys. Rev. Lett.* 91, 071301 (2003)
- [34] S. Das, P. S. Corasaniti and J. Khoury, *Phys. Rev. D* 73, 083509 (2006)
- [35] G.-B. Zhao et al., *Phys. Lett. B* 648, 8 (2007)
- [36] E. V. Linder and D. Huterer, *Phys. Rev. D* 72, 043509 (2005)
- [37] J. R. Bond, G. Efstathiou and M. Tegmark, *Mont. Not. Roy. Astron. Soc.*, 291, L33 (1997)
- [38] R. Bowen, S. H. Hansen, A. Melchiorri, J. Silk and R. Trotta, *Mont. Not. Roy. Astron. Soc.*, 334, 760 (2002); S. H. Hansen et al., *Phys. Rev. D* 65 023511 (2002)
- [39] G. L. Fogli et al., *Phys. Rev. D* 75, 053001 (2007); G. L. Fogli et al., *Phys. Rev. D* 70 113003 (2004)
- [40] W. H. Kinney, E. W. Kolb, A. Melchiorri and A. Riotto, *Phys. Rev. D* 74 023502 (2006)
- [41] L. Covi, J. Hamann, A. Melchiorri, A. Slosar and I. Sorbera, *Phys. Rev. D* 74 083509 (2006); J. Hamann, L. Covi, A. Melchiorri and A. Slosar, *Phys. Rev. D* 76 023503 (2007)
- [42] J. Larena et al., *in preparation*
- [43] G. R. Dvali, G. Gabadadze and M. Porrati, *Phys. Lett. B* 485, 208 (2000); C. De Ayet, *Phys. Lett. B* 502, 199 (2001)
- [44] A. Lewis and S. Bridle, *Phys. Rev. D* 66, 103511 (2002)